ISSN 2616-5880 Vol. 6, Issue 1: 36-43, DOI: 10.25236/AJMC.2025.060104

Upconversion Luminescence Modulation Based on Sandwich Structure with Interlayer Doping

Xinru Liu, Xiyan Zhu, Pei Jiang, Fei Li*

Hunan University of Science and Technology, Xiangtan, China
**Corresponding author*

Abstract: *Upconversion nanoparticles (UCNPs) as energy donors in luminescent resonance energy transfer (LRET) technology have shown broad prospects in various applications. To enhance the efficiency of LRET, this study designed and synthesized a sandwich-structured $NaYF_4@NaYF_4:Yb^{3+}/Er^{3+}@NaYF_4$ upconversion nanoparticle. This core-shell structure places the luminescent ions Er^{3+} in the inner shell, close to the nanoparticle surface, maintaining good proximity to the external energy acceptor. By adjusting the doping concentration in the intermediate layer, we successfully optimized the upconversion luminescence properties, regulating the emission wavelength and intensity. The results show that the luminescence efficiency of the sandwich-structured nanoparticles is significantly superior to that of the single $NaYF_4: Yb^{3+}/Er^{3+}$core nanoparticles, effectively improving their signal-to-noise ratio in sensor applications. This study provides stronger support for the application of UCNP-based LRET technology in temperature sensor design.*

Keywords: *Up-conversion luminescence; sandwich structure; temperature sensitivity*

1. Introduction

The nonlinear photonic upconversion process of combining two or more low-energy photons into a single high-energy photon, observed in lanthanide-doped nanomaterials,[1] has enabled a range of emerging applications from single-molecule detection and sensing,[2-5] in vivo bioimaging color- and lifetime-based optical multiplexing,[6-8]super-resolution imaging[9-11], and optical tweezers,[12,13]to volume displays and microcavity lasers. Their anti-Stokes photon upconversion process offers a number of superior advantages, including negligible autofluorescence background, narrow emission bandwidth, superior photostability, and deep-tissue penetration through near-infrared (NIR) optically transparent biological windows.[14,15]The photon upconversion process involves complex interactions, energy transfer processes, and internal and surface quenching pathways in the network of photon sensitizers and emitters, all of which are distance-dependent phenomena.[16,17]Therefore, the concentration of dopant ions plays a crucial role in determining the luminescent properties of upconversion nanoparticles (UCNPs). Varying the doping concentration of sensitizer and emitter ions can effectively increase the efficiency of the cascade energy transfer process, but it also short-circuits the sensitized photon energy to the bursting agent through cross-relaxation and non-radiative pathways. Therefore, the concentration-burst effect and the short-circuiting of excited-state energy to the surface bursting agent are considered to be the main mechanisms limiting UCNPs at relatively low doping concentrations, i.e., less than 20mol % for Yb^{3+} sensitizers, less than 1.5mol % for Er^{3+} activators, and less than 0.5mol % for Tm^{3+} activators.

Since the concentration burst threshold of the sensitizer or activator is highly dependent on the excitation power, it is crucial to determine the optimal concentration of sensitizer and emitter ions at any practical excitation power density, which is necessary for the development of high-brightness nanocrystals for various applications. Therefore, in this paper, a series of $NaYF_4@NaYF_4:x\%Yb^{3+}/1.5\%Er^{3+}@NaYF_4$ (core-sandwich-shell), also known as sandwich structure, was prepared by solvent-thermal method. The nanomaterials with high temperature sensitivity were prepared by adjusting the doping concentration of Yb^{3+} and observing the changes in luminescence intensity and color of the nanocrystals.

ISSN 2616-5880 Vol. 6, Issue 1: 36-43, DOI: 10.25236/AJMC.2025.060104

2. Experiment

2.1. Materials and characteristics

The rare earth oxides Y_2O_3 (99.99%), Yb_2O_3 (99.99%), and Er_2O_3 (99.99%) were purchased from Shanghai Second Chemical Reagents Factory. NaOH, NH_4F, NaF, hydrochloric acid, ethanol, methanol, ethylene glycol, and cyclohexane were provided by Sinopharm Chemical Reagent Co.,Ltd. (Shanghai). Oleic acid (OA) (90%) and 1-octadecene (90%) were purchased from Sigma-Aldrich. The corresponding metal oxides of YCl_3, $YbCl_3$, and $ErCl_3$ were dissolved in hydrochloric acid at high temperatures for preparation.

2.2. Experimental Steps

2.2.1. Synthesis of $NaYF_4$ Core

The synthesis was carried out using the solvothermal method. For the core preparation, 0.2mmol of YCl_3 aqueous solution was mixed with 10mL of oleic acid (OA) in a 50mL three-neck flask (A1). The mixture was heated to 165°C and maintained for 60 minutes. Then, 6mL of octadecene (ODE) was added, and the reaction was continued for 20 minutes before cooling to room temperature. Meanwhile, a methanol solution containing 5mmol NaOH, 3mmol NH_4F, 4mL OA, and 4mL octadecene was slowly added to a separate flask (B1). The mixture was heated to 110°C and maintained for 80 minutes before cooling to room temperature. Finally, the solution from flask (B1) was added to flask (A1), and the reaction was carried out under a nitrogen atmosphere at 300°C for 1 hour. Afterward, the mixture was cooled to 60°C and stored.

2.2.2. Synthesis of $NaYF_4$: Yb^{3+}/Er^{3+} inner-Shell

To synthesize the intermediate layer, the following procedure was adopted: First, a mixture of YCl_3 solution (x mmol = percentage * 0.2mmol), $YbCl_3$ solution (y mmol = percentage * 0.2mmol), and $ErCl_3$ solution (0.003mmol) was prepared in a 50mL three-neck flask (A2) with 10mL of oleic acid (OA). The mixture was then heated to 165°C under stirring and maintained for 60 minutes. Afterward, 6 mL of octadecene (ODE) was added, and the reaction continued for 20 minutes before cooling to room temperature. Meanwhile, in another flask (B2), a methanol solution containing 5mmol NaOH, 3mmol NH_4F, 4mL of OA, and 4mL of ODE was prepared. This solution was slowly added to flask (B2) and heated to 110°C for 80 minutes, followed by cooling to room temperature. After the reaction in flask (B2) was complete, the solution was added to flask (A2). The mixture was then heated to 300°C under a nitrogen atmosphere and maintained for 1 hour to allow the reaction to proceed. Afterward, the temperature was lowered to 60°C, and the intermediate layer (cladding layer) was obtained and stored at room temperature for further use. This method successfully forms the intermediate layer between the core and outer shell, ensuring a uniform and effective cladding structure for the final $NaYF_4$-based nanocrystals.

2.2.3. Synthesis of $NaYF_4$: Yb^{3+}/Er^{3+} Outer Shell

For the synthesis of the outer shell, the following procedure was carried out: First, a mixture of 0.2mmol YCl_3 solution and 10mL of oleic acid (OA) was prepared in a 50mL three-neck flask (A3). The mixture was then heated to 165°C with stirring and maintained for 60 minutes. Afterward, 6mL of octadecene (ODE) was added, and the reaction continued for an additional 20 minutes before cooling to room temperature. Meanwhile, in another flask (B3), a methanol solution containing 5 mmol NaOH, 3mmol NH_4F, 4mL of OA, and 4mL of ODE was prepared. This solution was slowly added to flask (B3), and the mixture was heated to 110°C for 80 minutes, followed by cooling to room temperature. After the reaction in flask (B3) was complete, the solution was transferred into flask (A3). The mixture was then heated to 300°C under a nitrogen atmosphere and maintained for 1 hour to allow the reaction to proceed. Afterward, the temperature was lowered to 60°C, and the outer shell was obtained and stored at room temperature for further use. This procedure successfully forms the outer shell layer of the $NaYF_4$-based nanocrystals, completing the core-shell structure necessary for enhanced upconversion fluorescence properties.

2.2.4. Synthesis of the Sandwich-structured $NaYF_4$@$NaYF_4$:Yb^{3+}/Er^{3+}@$NaYF_4$ Nanoparticles

The prepared $NaYF_4$ core, $NaYF_4$:Yb^{3+}/Er^{3+} inner shell, and $NaYF_4$ outer shell were added to a 50mL two-neck flask (C) containing 15mL of octadecene (ODE) and 15mL of oleic acid (OA). Nitrogen gas was continuously purged to exclude oxygen, and the mixture was stirred and heated to 165°C. This

ISSN 2616-5880 Vol. 6, Issue 1: 36-43, DOI: 10.25236/AJMC.2025.060104

temperature was maintained for 30 minutes to remove any water and oxygen in the solution, resulting in a uniform, clear, light yellow solution. Afterward, the temperature was raised to 215°C and maintained for a sufficient time to ensure the complete removal of any residual moisture. Finally, the solution was rapidly heated (within 15 minutes) to 315°C and kept at this temperature for 120 minutes. This step ensures the final annealing process, promoting the crystallization and uniformity of the core-shell nanoparticles. The high-temperature treatment at 315°C allows for the optimal formation of the sandwich-structured $NaYF_4$@$NaYF_4$:Yb^{3+}/Er^{3+}@$NaYF_4$ nanoparticles with improved fluorescence properties.

After the reaction, the temperature controller was turned off, and a brown transparent mixture was obtained. It was then allowed to cool to room temperature under a nitrogen atmosphere. The mixture was centrifuged at 10,000 rpm for 5 minutes to collect the brown-yellow product. The product was washed three times with cyclohexane, anhydrous ethanol, and deionized water. Finally, the product was dispersed in 10 mL of cyclohexane for future use.

3. Results and discussion

The upconversion luminescence emission spectra were recorded using a Hitachi F-2700 fluorescence spectrometer equipped with a tunable power infrared laser (980 nm), and the sample temperature was controlled by a temperature controller (REXC100FK02-V*AN). Upconversion luminescence images were captured using a camera. All experiments were conducted at room temperature.

3.1. Comparative analysis of three structures

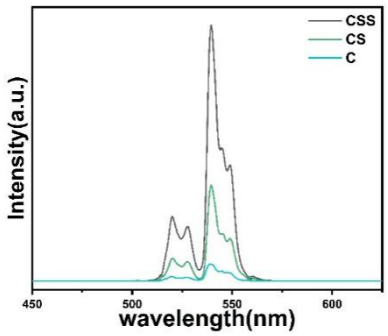

Figure 1: Comparison of upconversion luminescence intensity of $NaYF_4$:20%Yb^{3+}/1.5%Er^{3+}, $NaYF_4$:20%Yb^{3+}/1.5%Er^{3+}@$NaYF_4$, and $NaYF_4$@ $NaYF_4$:20%Yb^{3+}/1.5%Er^{3+}@$NaYF_4$

Figure 1 compares the upconversion luminescence intensities of three structures—$NaYF_4$:Yb^{3+}/Er^{3+}(core-C), $NaYF_4$:Yb^{3+}/Er^{3+}@$NaYF_4$ (core-shell-CS), and $NaYF_4$@ $NaYF_4$:Yb^{3+}/Er^{3+}@$NaYF_4$ (core-shell-shell-CSS)—under the same doping concentration and excitation power. In UCNPs, $NaYF_4$:Yb^{3+}/Er^{3+}core nanoparticles are the most classic structure for green light emission. In recent years, to enhance the luminescence intensity of the nanoparticles, shell layers are often coated to protect the energy transfer process and reduce energy loss. From the comparison shown in the figure, it is evident that the shell layers significantly improve the luminescence intensity of the nanoparticles.

3.2. Upconversion Luminescence Analysis

This study investigates the synthesis of luminescent sandwich-structured nanocrystals via a solvothermal method. The upconversion luminescence intensity of $NaYF_4$@NaYF4:Yb^{3+}/Er^{3+} @$NaYF_4$ nanocrystals was measured using a Hitachi FL2700 spectrophotometer under 980 nm laser excitation, while controlling other relevant parameters. The Yb^{3+} ions effectively absorb the 980 nm excitation light and transfer the energy to the Er^{3+} ions. A moderate concentration of Yb^{3+} helps to enhance the excitation rate of Er^{3+}, thereby increasing its luminescence intensity. However, as the Yb^{3+} concentration increases, concentration quenching effects may occur. At high concentrations of Yb^{3+}, the energy transfer efficiency decreases due to the enhanced interactions between Yb^{3+} ions, which can lead to energy transfer saturation.

As shown in Figure 2, in Yb^{3+}-doped nanocrystals, the emission process of Er^{3+} relies on the energy transfer mechanism between Yb^{3+} and Er^{3+}. When Yb^{3+} ions absorb 980 nm laser light, they undergo a

ISSN 2616-5880 Vol. 6, Issue 1: 36-43, DOI: 10.25236/AJMC.2025.060104

transition from the ground state ($^2F_{7/2}$) to the excited state ($^2F_{5/2}$). Then, the Yb^{3+} ions transfer their excited energy to the neighboring Er^{3+} ions via non-radiative relaxation or energy transfer processes. After absorbing this energy, Er^{3+} ions transition from the ground state ($^4I_{15/2}$) to higher excited states, and subsequently release the energy through different radiative transitions, producing light emission at specific wavelengths. Specifically, when Er^{3+} transitions from $^4S_{3/2}$ and $^2H_{11/2}$ to $^4I_{15/2}$, green light is emitted at wavelengths of 515-535 nm (centered at 520 nm) and 535-570 nm (centered at 540 nm). Meanwhile, the transition from $^4F_{9/2}$ to $^4I_{15/2}$ results in red light emission at wavelengths of 650-670 nm.

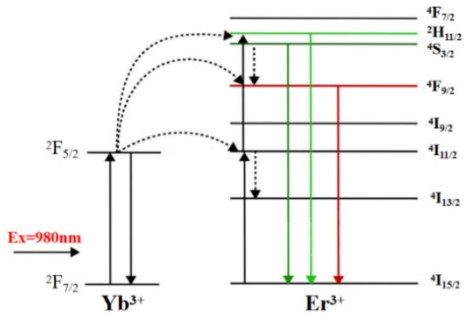

Figure 2: Energy level structure of Er^{3+} ions and their upconversion emission mechanism

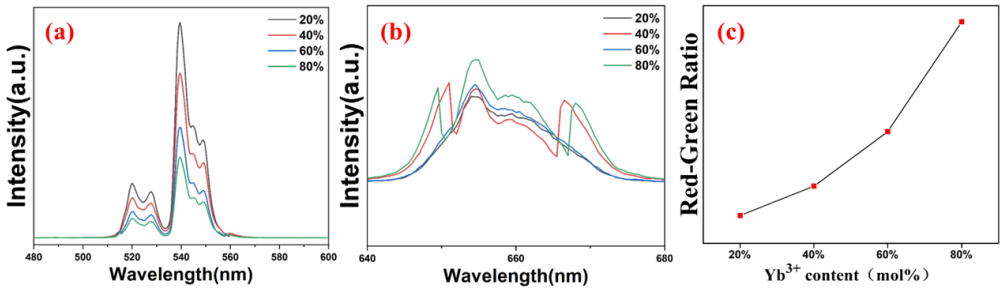

Figure 3: (a) Upconversion fluorescence spectra of $NaYF_4$@$NaYF_4$: Yb^{3+}/Er^{3+}@$NaYF_4$ at room temperature under 980 nm laser excitation, with different Yb^{3+} doping concentrations (20%, 40%, 60%, 80%) and a fixed Er^{3+} concentration of 1.5%.(b) Effect of different Yb^{3+} ion concentrations on the red-to-green emission intensity ratio

As shown in Figure 3(a)(b), the upconversion fluorescence spectrum of $NaYF_4$@$NaYF_4$: Yb^{3+}/Er^{3+}@$NaYF_4$ nanocrystals mainly consists of two emission bands. The green emission peak centered at 520 nm corresponds to the Er^{3+} $^2H_{11/2}\rightarrow{}^4I_{15/2}$ electronic transition, while the strong green emission peak centered at 540 nm originates from the Er^{3+} $^4S_{3/2}\rightarrow{}^4I_{15/2}$ electronic transition. Additionally, the red emission peak centered at 653 nm corresponds to the Er^{3+} $^4F_{9/2}\rightarrow{}^4I_{15/2}$ electronic transition. Since the emission peaks of UCNPs are centered at 520 nm and 540 nm, which dominate the visible range of the fluorescence spectrum, bright green light can be observed by the naked eye.

As observed in Figure 3(c), under 980 nm near-infrared laser excitation, the red-to-green emission ratio of the nanocrystals increases with the concentration of Yb^{3+}, and the emission color gradually shifts from green to yellow. Yb^{3+} ions serve as an effective light sensitizer, efficiently absorbing the excitation light and transferring its energy to Er^{3+} ions. The increase in Yb^{3+} concentration enhances the fluorescence intensity of $NaYF_4$. As the Yb^{3+} concentration increases, the excitation capability of Yb^{3+} enhances, which in turn increases the emission from Er^{3+}. This emission is primarily a combination of red and green light. However, with the increase in Yb^{3+} ion concentration, the redistribution of the emission spectrum or competition between different emission energy levels occurs, leading to the enhancement of specific wavelengths of light (such as red light), causing the overall emission color to shift toward yellow. To make this effect more visually intuitive, photographs of the $NaYF_4$@$NaYF_4$: Yb^{3+}/Er^{3+}@$NaYF_4$ nanocrystals were taken, as shown in Figure 4.

ISSN 2616-5880 Vol. 6, Issue 1: 36-43, DOI: 10.25236/AJMC.2025.060104

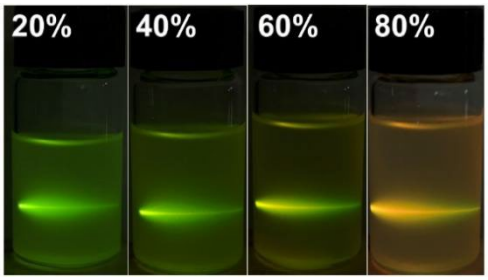

Figure 4: Photographs of the luminescence of $NaYF_4$@$NaYF_4$: Yb^{3+}/Er^{3+}@$NaYF_4$ nanocrystals, doped with different concentrations of Yb^{3+}, dispersed in cyclohexane solution under 980 nm laser irradiation (with the same nanoparticle concentration)

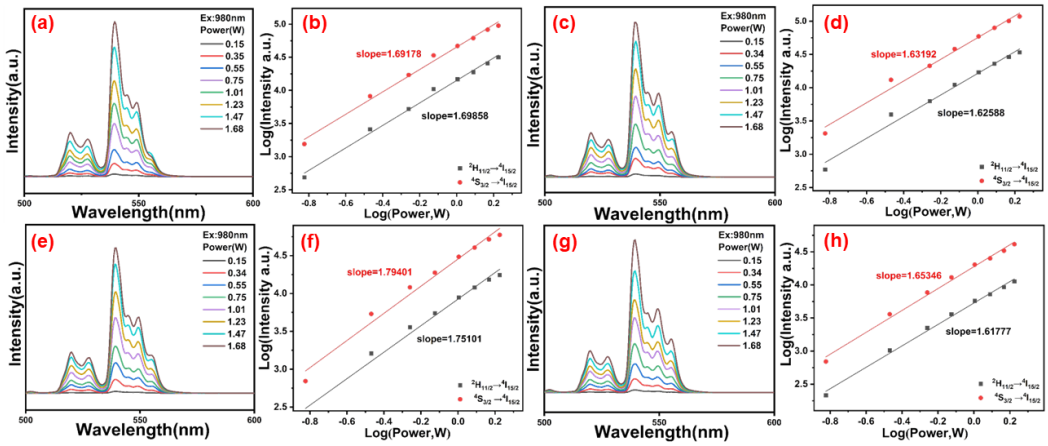

Figure 5: (a) (c) (e) (g) Luminescence spectra of CSS structures at different Yb^{3+} ion concentrations corresponding to excitation power densities of 0.15 ~ 1.47 W/cm2; (b) (d) (f) (h) Green light emission intensity (520 nm, 540 nm) versus excitation power for $NaYF_4$@$NaYF_4$: x%Yb^{3+}/1.5%Er^{3+}@$NaYF_4$ (x=20,40,60, 80 mol%) nanoparticles with green light emission intensity (520 nm,540 nm) versus excitation power

Figure5.(b)(d)(f)(h)shows the evaluation of power dependent emission intensity at 980 nm for $NaYF_4$@$NaYF_4$:Yb^{3+}/Er^{3+}@$NaYF_4$nanoparticles. Where, (a)(c)(e)(g)shows the luminescence spectra of the CSS structure at excitation power densities of 0.15~1.47W/cm^2 for $NaYF_4$@$NaYF_4$:Yb^{3+}/Er^{3+}@$NaYF_4$nanoparticles. The spectra consist of characteristic emission peaks from the Er^{3+} transitions: $^2H_{11/2}\rightarrow{}^4I_{15/2}$ (520 nm) and $^4S_{3/2}\rightarrow{}^4I_{15/2}$ (540 nm). By analyzing the peak intensities at 520 nm and 540 nm under 980 nm laser excitation, the power dependence of the $^2H_{11/2}\rightarrow{}^4I_{15/2}$ (520 nm) and $^4S_{3/2}\rightarrow{}^4I_{15/2}$ (540 nm) energy levels is shown. Increasing the excitation power raises the photon density, which enhances the energy transfer processes within the nanocrystals, making the luminescence intensity positively correlated with the excitation power.

3.3. Sensitivity Analysis of Temperature Measurement of Sandwich Structure

To explore the temperature sensing properties of $NaYF_4$@$NaYF_4$: $Yb^{3+/}Er^{3+}$@$NaYF_4$upconversion nanoparticles and their potential applications in high-sensitivity and precise temperature measurement, the nanoparticles were heated to a set temperature using a heating stage. The emission spectra of $NaYF_4$@$NaYF_4$: 20%Yb^{3+}/1.5%Er^{3+}@$NaYF_4$ were measured under 980 nm near-infrared laser excitation at different temperatures. By comparing the fluorescence intensity at different temperatures in Figure 6(a), the trend of fluorescence intensity change with temperature can be observed. This trend allows for the assessment of the temperature sensor's sensitivity. The fluorescence intensity at different temperatures can be well fitted, and this process follows the Boltzmann distribution, indicating that the temperature-related luminescence intensity variation adheres to the expected physical model for thermally activated processes.

$$FIR = \frac{I_{520}}{I_{540}} = A \cdot exp\left(-\frac{\Delta E}{k_B T}\right) = A \cdot \exp\left(-\frac{b}{T}\right), \quad (1)$$

where A is a constant determined by the UCNP is, b = ΔE/kB, ΔE refers to the energy level gap between $^4H_{11/2}$ and $^4S_{3/2}$, kB denotes the Boltzmann constant, and T denotes the absolute temperature.

ISSN 2616-5880 Vol. 6, Issue 1: 36-43, DOI: 10.25236/AJMC.2025.060104

The temperature dependence of the FIR can be derived from a good fit of Eq. (1). As shown in Figure. 6(b), demonstrating the relationship between Ln(FIR) and the temperature reciprocal:

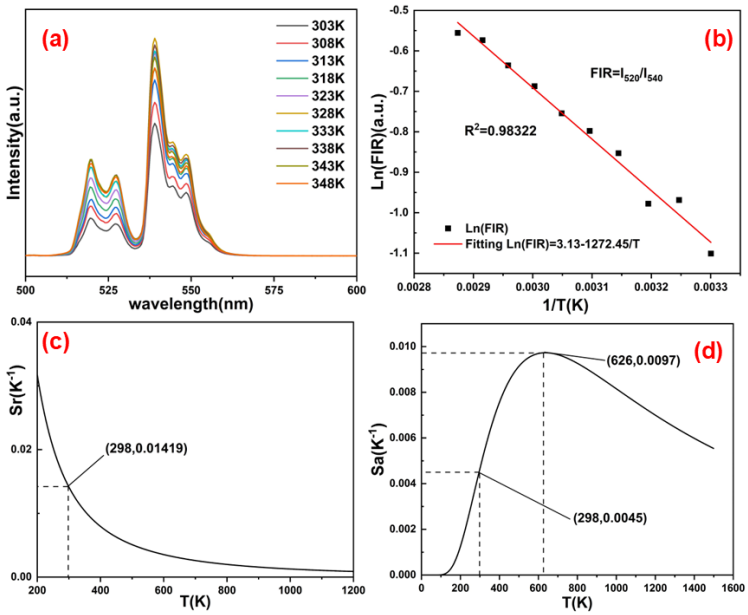

Figure 6: (a) Fluorescence emission spectra of $NaYF_4$@$NaYF_4$: 20% Yb^{3+}/1.5% Er^{3+}@$NaYF_4$ at different temperatures; (b) Experimental results of FIR natural logarithm versus temperature inverse variation; (c) Relative sensitivity versus temperature variation; (d) Absolute sensitivity versus temperature variation.

Sensitivity S is an important index to characterize the performance of optical thermal response, which is divided into relative sensitivity (Sr) and absolute sensitivity (Sa), where the absolute sensitivity indicates the change of FIR with temperature, and the absolute sensitivity is the normalized expression of the relative sensitivity, so the relative sensitivity and absolute sensitivity are respectively defined as

$$S_r = \left|\frac{1}{FIR}\frac{\partial FIR}{\partial T}\right| = b/T^2, \quad (2)$$

$$S_a = \left|\frac{\partial FIR}{\partial T}\right| = FIR \times b/T^2, \quad (3)$$

where FIR is the fluorescence intensity ratio at temperature T. It is worth noting that active biological tissues have higher biological activity in the temperature range of 273K-333K, and 298K is the room temperature in this temperature range, so it is necessary to investigate the performance of the optical nanothermometer at 298K, and the relative and absolute sensitivities were calculated by Eq. (2) and Eq. (3), and the relative and absolute sensitivities in the $NaYF_4$@$NaYF_4$: Yb^{3+}/Er^{3+}@$NaYF_4$ upconversion nanoparticles at 298 K. The relative and absolute sensitivities of the nanoparticles are 14.19 $\times 10^{-3}K^{-1}$ and $4.5\times10^{-3}K^{-1}$, respectively (Fig. 6(c)(d)); when the temperature reaches 626 K, the relative sensitivity of the nanosystem reaches the maximum value, viz, Samax = $9.7\times10^{-3}K^{-1}$ (Fig. 6(d)).

4. Conclusion

The sandwich-structured nanocrystals offer a range of performance advantages through their unique layered design and combination, making them suitable for a wide array of technological and application fields. In this study, $NaYF_4$@$NaYF_4$: Yb^{3+}/Er^{3+}@$NaYF_4$ nanocrystals were successfully synthesized using a solvothermal method, and their properties were analyzed through a series of characterizations and tests.

The $NaYF_4$ core, coated with a $NaYF_4$ intermediate layer doped with $Yb^{3+}$and $Er^{3+}$and an outer $NaYF_4$ shell, forms a well-organized layered structure that facilitates effective energy transfer and luminescence. The $NaYF_4$ core provides a stable crystal structure, ensuring the stability of the nanoparticle. The intermediate layer, which is doped with $Yb^{3+}$and Er^{3+}, plays a crucial role in the energy transfer process: Yb^{3+}absorbs near-infrared light as an effective sensitizer and transfers the energy to Er^{3+}, enabling visible light emission. The doping in the inner shell helps reduce non-radiative transitions caused by surface defects, improving energy utilization efficiency. The emission wavelength and intensity can be optimized

ISSN 2616-5880 Vol. 6, Issue 1: 36-43, DOI: 10.25236/AJMC.2025.060104

by adjusting the doping concentration. The outer $NaYF_4$ shell serves to protect the intermediate and core layers from external environmental influences, providing additional stability and durability, ensuring consistent performance over extended use. The three-layer structure of $NaYF_4$@$NaYF_4$: Yb^{3+}/Er^{3+}@$NaYF_4$ works synergistically: the core offers fundamental stability, the intermediate layer is responsible for efficient energy absorption and upconversion luminescence, and the shell protects and enhances optical performance. By varying the excitation power, it was found that as the excitation light power increases, the energy transfer process inside the nanoparticle becomes more efficient, effectively improving the signal-to-noise ratio (SNR) in sensor applications. Using fluorescence intensity ratio techniques, the temperature-sensing properties of the nanoparticles doped with 20% Yb^{3+} were studied, providing strong support for future high-performance temperature measurement technologies.

Acknowledgements

Data Availability: Data supporting the results of this study are available upon request from the first author.

References

[1] Vennerberg, D., & Lin, Z. (2011). Upconversion nanocrystals: synthesis, properties, assembly and applications. Science of Advanced Materials, 3(1), 26-40.
[2] Tanaka, R., Kitagawa, Y., & Shinozaki, K. (2023). Effect of adding Er^{3+} on the precipitated crystalline phase of SrF_2–ZnO–B_2O_3 glass and upconversion luminescence. Optical Materials: X, 20, 100268.
[3] Gocmen, M. S., & Dulda, A. (2024). Effect of Pr^{3+} concentration in luminescence properties & upconversion mechanism of triple doped NaYF4: Yb^{3+}, Er^{3+}, Pr^{3+}. Methods and Applications in Fluorescence, 12(2), 025006.
[4] Mettenbrink, E. M., Yang, W., & Wilhelm, S. (2022). Bioimaging with upconversion nanoparticles. Advanced photonics research, 3(12), 2200098.
[5] Li, Y., Chen, C., Liu, F., & Liu, J. (2022). Engineered lanthanide-doped upconversion nanoparticles for biosensing and bioimaging application. Microchimica Acta, 189(3), 109.
[6] Sun, Q. C., Ding, Y. C., Sagar, D. M., & Nagpal, P. (2017). Photon upconversion towards applications in energy conversion and bioimaging. Progress in Surface Science, 92(4), 281-316.
[7] Mader, H. S., Kele, P., Saleh, S. M., & Wolfbeis, O. S. (2010). Upconverting luminescent nanoparticles for use in bioconjugation and bioimaging. Current opinion in chemical biology, 14(5), 582-596.
[8] Lin, M., Cheng, S., Wu, X., Zhan, S., & Liu, Y. (2021). Optical temperature sensing based on upconversion nanoparticles with enhanced sensitivity via dielectric superlensing modulation. Journal of Materials Science, 56, 10438-10448.
[9] Gao, W., Han, S., Wang, B., Sun, Z., Lu, Y., Han, Q., ... & Dong, J. (2022). Single-layer gold nanoparticle film enhances the upconversion luminescence of a single $NaYbF_4$:2%Er^{3+} microdisk. Journal of Alloys and Compounds, 900, 163493.
[10] Lu, D., Retama, J. R., Marin, R., Marqués, M. I., Calderón, O. G., Melle, S., ... & Jaque, D. (2022). Thermoresponsive polymeric nanolenses magnify the thermal sensitivity of single upconverting nanoparticles. Small, 18(34), 2202452.
[11] Back, M., Ueda, J., Brik, M. G., & Tanabe, S. (2020). Pushing the limit of Boltzmann distribution in Cr^{3+}-doped $CaHfO_3$ for cryogenic thermometry. ACS applied materials & interfaces, 12(34), 38325-38332.
[12] Mykhaylyk, V., Kraus, H., Zhydachevskyy, Y., Tsiumra, V., Luchechko, A., Wagner, A., & Suchocki, A. (2020). Multimodal non-contact luminescence thermometry with Cr-doped oxides. Sensors, 20(18), 5259.
[13] Back, M., Casagrande, E., Brondin, C. A., Ambrosi, E., Cristofori, D., Ueda, J., ... & Riello, P. (2020). Lanthanide-doped Bi_2SiO_5@ SiO_2 core–shell upconverting nanoparticles for stable ratiometric optical thermometry. ACS Applied Nano Materials, 3(3), 2594-2604.
[14] Liu, H., Kulkarni, A., Kostiv, U., Sandberg, E., Lakshmanan, A., Sotiriou, G. A., & Widengren, J. (2024). Interplay between a Heptamethine Cyanine Dye Sensitizer (IR806) and Lanthanide Upconversion Nanoparticles. Advanced Optical Materials, 12(29), 2400987.
[15] Zhao, T., Wu, D., Zhang, X., & Lyu, H. (2024). A fluorescent sensor based on single band bright red luminescent core-shell UCNPs for the high-sensitivity detection of glucose and glutathione.Analytica Chimica Acta, 1295, 342323.
[16] Konugolu Venkata Sekar, S., Ma, H., Komolibus, K., Dumlupinar, G., Mickert, M. J., Krawczyk, K.,

ISSN 2616-5880 Vol. 6, Issue 1: 36-43, DOI: 10.25236/AJMC.2025.060104

& Andersson-Engels, S. (2024). High contrast breast cancer biomarker semi-quantification and immunohistochemistry imaging using upconverting nanoparticles. Biomedical Optics Express, 15(2), 900-909.

[17] Dubey, N., Gupta, S., Shelar, S. B., Barick, K. C., & Chandra, S. (2024). Maximizing Upconversion Luminescence of Co-Doped CaF_2: Yb, Er Nanoparticles at Low Laser Power for Efficient Cellular Imaging. Molecules, 29(17), 4177.